


INFORMATION SCIENCE

Millimeter-scale fluid-driven soft robots

Rong Bian¹, Ningbin Zhang¹, Xinyu Yang¹, Jinhao Li¹, Dezhi Yang¹, Jieji Ren¹,
Jiang Zou^{1,2} and Guoying Gu ^{1,2,*}

ABSTRACT

Millimeter-scale soft robots (milli-SRs) promise significant advancements in biomedical engineering and inspection, enabling precise navigation in confined spaces. However, fabricating miniaturized fluid-driven soft robots is hindered by microscale forces. Here, we introduce a new universal design and fabrication approach (referred to as the mini bubble casting method) to create high-quality multifunctional fluid-driven milli-SRs. By injecting a bubble into pre-modified silicone liquid under high-stability conditions, we achieve submillimeter internal voids, overcoming interfacial-tension-induced instability. The modification strategy is guided by our theoretical model, which explains the influence of viscous resistance and interfacial tension on the dynamic behavior of the bubble-silicone interface. We successfully fabricate soft milli-actuators ten times smaller than existing works with low surface smoothness ($R_a = 11.2$ nm). We demonstrate a milli-gripper handling delicate insects and a thrombus extractor for narrow vessels. We present a miniature steerable tip for bronchial navigation, improving safety and dexterity over traditional tools, showing the tremendous biomedical potential of these devices.

Keywords: soft robotics, miniaturized robot, fluid dynamic, biomedical tool

INTRODUCTION

Millimeter-scale soft robots (milli-SRs), ranging from several millimeters down to hundreds of micrometers in size, are emerging as innovative tools in biomedical engineering and tissue inspection [1–7]. These robots can navigate through organs [1,8], grip objects [9,10] and transport medical devices and drugs [11] for diagnostics and therapy, offering minimally invasive access to natural body cavities (Fig. 1a). Milli-SRs can be actuated by various mechanisms, including pressure [12,13], an electric field [14,15], a magnetic field [16–18], a chemical reaction [19,20], light [21] and ultrasound [22]. Among these, fluid-driven robots are particularly prevalent due to their ease of control and robustness [23–26]. A typical fluid-actuated soft robot comprises the silicone elastomer with one or more internal voids [27]. The pressure change in voids can be converted into deformation of soft robots. For biomedical applications, fluid-driven milli-SRs without external magnetic sources, enabling compact, lightweight medical devices [28]. Fabricated by non-metallic, MRI-compatible materials, they eliminate image artifacts and enhance safety for both clinicians

and patients [29,30]. Consequently, they are well suited for complex endoluminal interventions [4], high-precision positioning [31] and environmental sensing [32] akin to magnetically driven milli-SRs.

While fluid-driven silicone robots at the centimeter scale are widely manufactured [33], fabricating their millimeter-scale counterparts remains challenging [34,35], especially in terms of robustness and stability, due to difficulties in creating smaller internal voids.

Structural defects and incompleteness frequently hinder the formation of millimeter-scale structures in traditional silicone molding methods. That is because the gravity and inertial forces, which dominate the molding process, are negligible compared to microscale forces in the low-Reynolds-number regime [35,36]. For example, in molding structures with a characteristic size of 1 mm, the Reynolds number is approximately 10^{-3} . In this case, gravity fails to drive the silicone into the mold, and buoyancy is insufficient to lift the entrapped air. Moreover, the shapes and dimensions of robotic structures are restricted by the challenges associated with extracting long, narrow molds from the cured silicone [37]. Lately,

¹State Key Laboratory of Mechanical System and Vibration, School of Mechanical Engineering, Shanghai Jiao Tong University, Shanghai 200240, China and ²Shanghai Key Laboratory of Intelligent Robotics, Shanghai Jiao Tong University, Shanghai 200240, China

*Corresponding author. E-mails: guguoying@sjtu.edu.cn

Received 16 April 2025; Revised 20 August 2025;

Accepted 10 September 2025

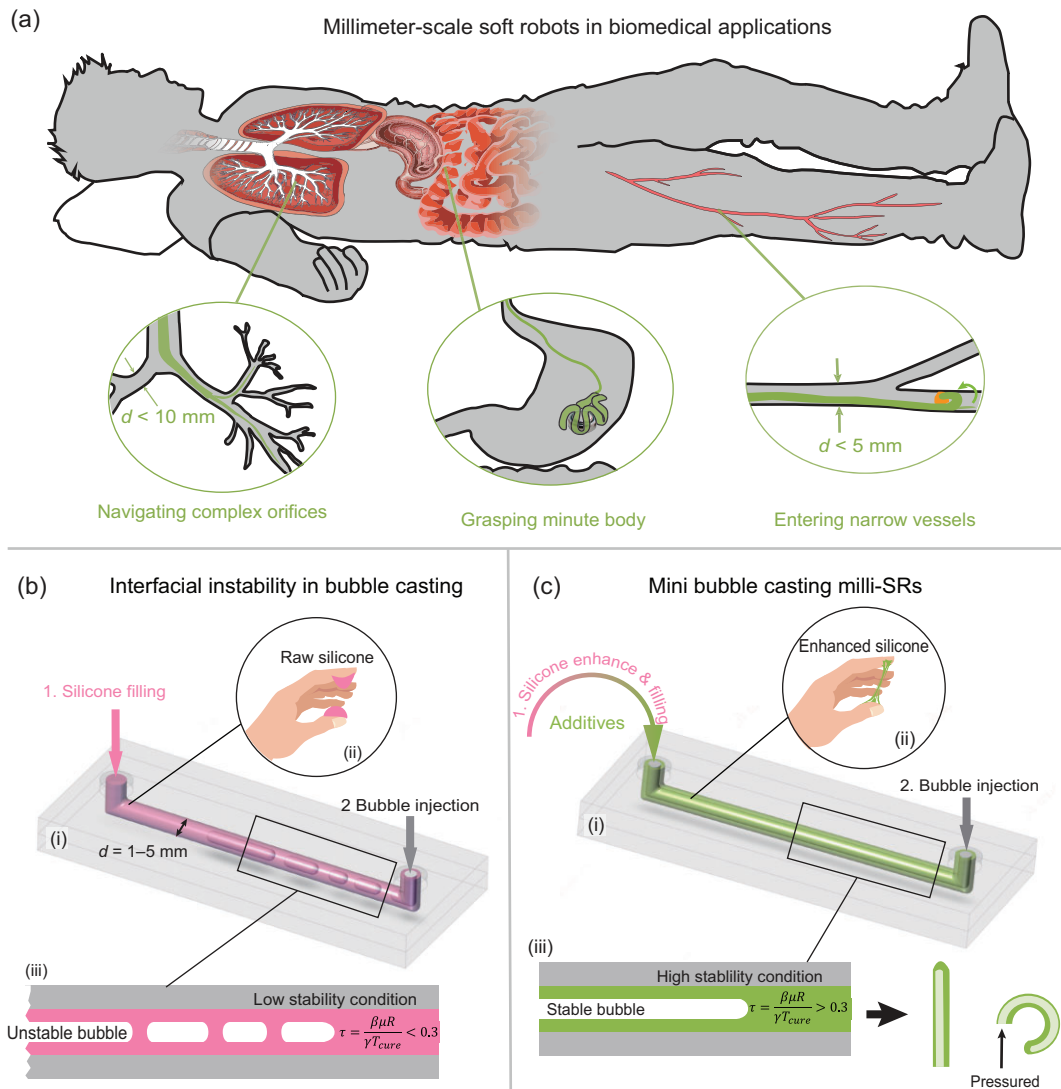


Figure 1. Concepts of milli-SRs and a comparison between bubble casting and mini bubble casting. (a) Milli-SRs take on biomedical tasks in confined and narrow human cavities, including navigating complex orifices, extracting foreign objects and entering narrow vessels. (b) Interfacial instability in bubble casting milli-SRs. The bubble is injected into the raw silicone liquid to form a robot void. When the robot size is scaled down to the millimeter scale, the unmodified raw commercial silicone presents a low stability condition and cannot resist the microscale forces such as surface tension, resulting in interfacial instability. (c) Mini bubble casting enables the robust fabrication of millimeter-scale soft robots by enhancing silicone stability through incorporating additives, following universal strategies guided by our theoretical model. The enhanced silicone liquid, under a high stability condition, exhibits resistance to interfacial tension and the bubble remains stable until the milli-SRs are formed.

other fabrication methods have been developed to enable novel mechanisms for mitigating failures induced by microscale forces; however, they encounter other problems. Three-dimensional (3D) printing faces limitations in material selection [38,39], and the film coating technique is also restricted to relatively simple geometries [40].

Recently, bubble casting [41] has emerged as a robust stable fabrication technique for manufacturing soft robots (Fig. 1b, i). It leverages the interfacial flow within silicone liquid to create elongated robot voids [42,43]. First, the liquid silicone is filled

into a tubular mold, followed by bubble injection where the air is injected to form a long bubble in the silicone. The ideal scenario is that the bubble stabilizes under mechanical equilibrium between viscous resistance, surface tension and gravity. However, maintaining the stability of the bubble-silicone interface at the millimeter scale presents significant challenges. In experiments, we observe that the bubble fragments into a few discrete bubbles, and the silicone converges into peaks and forms bridges (Fig. 1b, iii) and Movie S1), which limits its ability to fabricate millimeter-scale robots. We hypothesize

that this can be attributed to interfacial tension (Fig. 1b, ii), which increases rapidly as the scale decreases, becoming significantly greater than the viscous resistance of silicone and gravity, thereby causing an imbalance in mechanical equilibrium [44–46]. This study elucidates the mechanism of interfacial instability and its mitigation method. Whereas conventional bubble casting [41] centers on bubble forming, our focus is on the milli-bubble fragmentation and on devising a robust strategy for the reliable fabrication of fluid-driven milli-SRs.

Herein, we present a novel universal robust fabrication method, mini bubble casting (mini BC) to create fluid-driven silicone-based milli-SRs using various commercial liquid silicones (Fig. 1c), extending the lower size limit of the bubble casting process. To explore the dynamic behavior of silicone liquid at the millimeter scale, we establish a theoretical model and identify the influence of the curing time, viscous resistance and interfacial tension on the interfacial instability. Based on the model, a rheological stability condition τ is established and a universal modification strategy is proposed to enhance interfacial stability (Fig. 1c, iii) by incorporating commercially available additives. The enhanced silicone $\tau > 0.3$ can withstand interfacial tension (Fig. 1c, ii), enabling theoretical minimal diameters of 0.2 mm. To illustrate its efficacy, a variety of soft actuators with different shapes and actuation modes are created, featuring dimensions one order of magnitude smaller than existing works [41,42], outer diameters ranging from 1.0 to 3.0 mm and ultra-low surface roughness ($R_a = 11.2$ nm). We further demonstrate the capability of milli-SRs in interacting with delicate objects and navigating narrow natural human orifices, including a compliant and biosafe insect gripper and thrombus extractor for vascular interventional surgery. Additionally, we present a miniature flexible steerable tip with omnidirectional bending capability of up to 180° that can navigate complex bronchial environments and reach the quaternary bronchus, showcasing superior safety and dexterity compared to traditional medical tools. The proposed mini bubble casting affords novel possibilities for fabricating soft robots at the millimeter scale, unlocking numerous potential applications in biomedical fields.

RESULTS

Interfacial instability in bubble casting

To demonstrate its broad relevance, we conduct preliminary experiments and observe interfacial instability across various commercially available liquid silicones, including the VPS series commonly used

in bubble casting milli-SRs of varying diameters, as well as Ecoflex 30 and Dragon Skin 10 that are widely utilized in soft robotics laboratories (Fig. 2a).

The interfacial instability can be categorized into four distinct stages; see Fig. 2b. Initially, in stage 1, the bubble undergoes subtle unevenness near point A, and then it forms a notable ‘hill’ in stage 2. The silicone continues converging to point A and the bubble is on the verge of fracture during stage 3. Ultimately, the silicone bridges form and the long bubble fragments into several smaller, isolated bubbles in stage 4, which marks the failure of bubble casting milli-SRs.

To model the dynamic behaviors, we first consider why silicone liquid converges to point A. In Fig. 2c, the unevenness near point A creates a difference between the height of silicone layer at point A and point B, assuming that $h_A - h_B > 0$. The Young–Laplace formula dictates that surface tension generates a pressure differential at point A, quantified as (see the section entitled ‘Young-Laplace formula’)

$$P_A - P_B = \gamma \left(\frac{1}{R - h_B} - \frac{1}{R - h_A} \right) < 0, \quad (1)$$

where α is the surface tension coefficient between the silicone liquid and bubble, and R is the mold’s inner radius. Given that $P_A - P_B < 0$, the pressure gradient creates a pressure trap at point A that becomes deeper as h_A increases. This places the interface in an unstable equilibrium, triggering subsequent instability at the bubble-silicone interface.

Then the silicone flow behavior can be obtained by formulating dynamic equations (see the section entitled ‘Navier-Stokes equation’) that, during stages 1–3, yield

$$\frac{h_A}{h_0} = \left(1 - \frac{\alpha \gamma h_0}{2\pi^2 R^2 \mu} t \right)^{-n}, \quad (2)$$

$$T_{grow} \approx \frac{2\pi^2 \mu}{\alpha \gamma} \times \frac{R}{h_0} \times R, \quad (3)$$

where T_{grow} is the instability timespan, h_0 is the initial height of the silicone layer at point A, μ is the silicone viscosity. This progression stops when $h_A = R$ at stage 4, where the hill’s height reaches its maximum, breaking up the bubble. Figure 2d shows the growth of the dimensionless hill height h_A/h_0 over time for various diameters and silicone types, demonstrating close agreement with the theoretical Equation (2).

According to the model results, the interfacial instability is highly dependent on size and the rheological properties of the silicone liquid. The instability timespan T_{grow} is positively correlated with scale R . Furthermore, the growth velocity of height h_A correlates positively with the surface tension

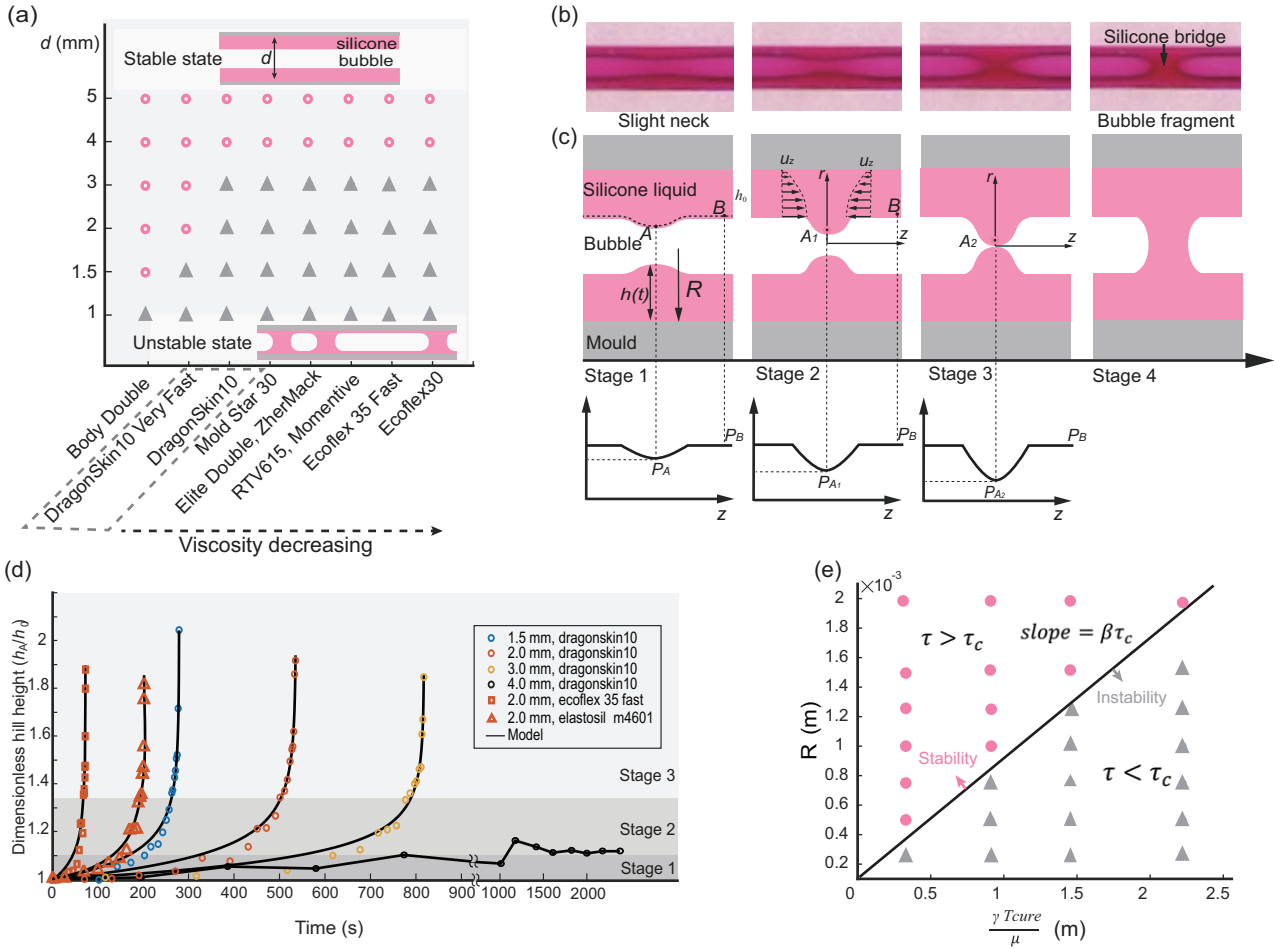


Figure 2. Model of interfacial instability. (a) Instability can be observed in the various commercial liquid silicones, including the VPS series used in bubble casting, as well as Ecoflex 30 and Dragon Skin 10 widely used in soft robotics laboratories. Silicones are arranged in descending viscosity; those of identical viscosity are grouped within dashed boxes. Their viscosities span 3–100 Pa s and cover the majority of commercially available silicones. (b) Four stages of interfacial instability from left to right. Diameter: 1.5 mm. (c) Diagram of silicone flow during the instability model, depicting the cross section of the silicone liquid (pink) and the bubble (white) within a tubular mold (gray). At point A, the formation of a silicone hill creates a pressure trap, which subsequently induces the convergence of the surrounding silicone. (d) Dimensionless hill height $h_A(t)/h_0$ versus time ($t = 0$ at bubble inception) for various diameters. The silicone liquid is Dragon Skin 10 (Smooth On Inc.), Ecoflex 35 Fast (Smooth On Inc.) and Elastosil M4601 (Wacker Inc.). Solid lines correspond to (2) with fitted parameters (mean \pm SE): Dragon Skin 10, $n = 0.0986 \pm 0.005$ and $\alpha = 0.12 \pm 0.04$; Ecoflex 35 Fast, $n = 0.112 \pm 0.006$ and $\alpha = 0.12 \pm 0.02$; Elastosil M4601, $n = 0.103 \pm 0.001$ and $\alpha = 0.13 \pm 0.01$. Parameter explanation and the fitting method are given in the section entitled ‘Explanation of the fitting parameters’ in [Supplementary data](#). (e) Occurrence of the interfacial instability under varying silicone conditions and within molds of different radii. Filled circles indicate stability and filled triangles indicate instability. The solid line classifies two states with the slope $\beta\tau_{th}$.

coefficient γ , and inversely with viscosity μ . This explains the antagonistic effects of surface tension (promoting instability) and viscous forces (inhibiting instability).

Instability condition and modification strategy

Determining whether instability occurs is another important aspect. To establish the instability condition, thought experiments are needed. It is noted that silicone liquid undergoes a viscosity increase and solidification during instability. Extreme stability

happens when the silicone curing time T_{cure} is significantly shorter than the instability timespan T_{grow} , causing the silicone to instantly freeze after bubble creation. Conversely, another scenario of extreme instability is where T_{grow} is so small that the instability occurs rapidly in the uncured silicone. Therefore, the stability condition, denoted τ , can be established as

$$\tau = \frac{T_{grow}}{T_{cure}} = \frac{\beta\mu R}{\gamma T_{cure}}, \quad (4)$$

where $\beta = (2\pi^2/\alpha) \times (R/h_0) \approx 329$. A large τ indicates high stability, while a small τ corresponds

to significant instability. Experiments validate the stability condition (Fig. 2e) and the threshold criterion can be calculated as $\tau_{th} = 0.3$ (see the subsection entitled ‘Stability condition’ in the Methods section below). The fabrication yield of mini bubble casting is quantified across various instability conditions and diameters (radius = 0.5–2.5 mm) to show the scalability of the proposed fabrication method. The improved fabrication yields confirm the scalability of the modification strategy (Fig. S3).

Based on the stability condition, we can increase the viscosity μ and decrease the curing time T_{cure} until $\tau > \tau_{th}$ to mitigate interfacial instability. Notably, considering that the excessively high viscosity and rapid curing of silicone are detrimental to the operational process, the upper limitation of viscosity, μ_{max} , is 100 Pa s and the low limitation of the curing time, $T_{cure,min}$, is 10 min, which means that the theoretical minimal diameter $d_{min} = 0.2$ mm (see the section entitled ‘Theoretical minimal diameter by mini-BC’).

Figure 3a shows the modification strategy. Firstly, the commercial additives, thickeners and accelerators are inserted into part A of silicone before both components are canned to injection cartridges. Taking the fabrication of 1.5-mm soft actuators with Dragon Skin 10 as an example, the unmodified silicone has a condition of $\tau_0 \approx 0.05$. Based on sheets from suppliers, we insert the thickener (Thi-Vex, Smooth-On Inc., 3% of part A) and the accelerator (Plat-Cat, Smooth-On Inc., 1% of part A in weight) into silicone A. The new condition in the mixed silicone liquid is $\tau \approx 0.4$. Then, the modified silicone is mixed in the mixing nozzle and injected into the mold. After a waiting period, the air is injected from another side and forms a long bubble in the silicone liquid. Figure 3b shows the interfacial behaviors under different conditions. Silicone with high τ shows interfacial stability. The process is shown in Movie S2. For other commercial silicone, the suggested additives and their dosage are listed in Table S1. Excluding silicone curing, total fabrication requires 10 min; including curing, the process spans 20–70 min (Table S2).

Milli-SRs by mini bubble casting

We successfully fabricated various milli-SRs that are similar but an order of magnitude smaller than those made by bubble casting. To demonstrate the stability of mini BC, a contractile coiling soft actuator ($R = 0.75$ mm, $L = 300$ mm) with aspect ratio L/R as high as 400 is created in Fig. 3c and Movie S3 (its counterpart $R = 5$ mm in bubble casting). Its con-

tractile ratio of original length to minimal length can reach up to 8.5 times and it generates a contractile force of ≈ 400 mN (Fig. S8). This millimeter-scale actuator can serve as a driver for micro-mechanical systems, analogous to the role of an electric motor in large-scale machinery. The contractile milli-actuator drives a microscale rotating pair lifting a minuscule paper clip (Fig. 3d and Movie S3). The bending milli-actuator spins a milli-gear set (Fig. 3e and Movie S4). We also create similar but smaller five-point star-shaped anisotropic actuators (Fig. 3f and Movie S5) and cross-like actuators (Fig. S2 and Movie S6). They are 10 mm in diameter and one order of magnitude smaller than their bubble-casting counterpart in size (80 mm in diameter).

The surface roughness of milli-SRs is measured at $R_a = 11.2$ nm using an atomic force microscope (MFP-3D, Oxford Instruments) equipped with a stylus tip radius of 1.0 μm , as shown in Fig. 3g. The roughness is several orders of magnitude smaller than its counterpart fabricated by casting ($R_a = 1$ – 10 μm [47]) and 3D printing ($R_a = 6$ μm [38]). We quantitatively evaluate the wall-thickness uniformity (Fig. S4); details to ensure consistency are provided in the section entitled ‘The uniformity of the robot’s wall thickness’. The milli-SRs withstand a thousand loading cycles without any visible degradation in deformation performance (see the section entitled ‘Motion repeatability’ and Fig. S6). Mini bubble casting is benchmarked against alternative fabrication routes in the section entitled ‘Comparative benchmarking of millimeter-scale fabrication techniques’.

Because of their delicacy and inherent safety, the milli-actuators are proficient in grasping tiny objects and entering narrow tubes. A soft bending actuator with a diameter of 1.5 mm can function as a milli-gripper of microscale objects that are easily deformed and damaged by rigid grippers. The ant model is gripped and held without damaging its body (Fig. 3g). Dislodgement of the ant from the milli-gripper requires a pulling force of ≈ 220 mN (Fig. S8). We can also create a soft milli-hook whose tip easily bends and body hardly deforms under a single pressure by programming the mini-BC process (Fig. S7). The hook penetrates the narrow canal, engages the foreign object and withdraws it intact (Fig. 3j; Movie S7). Free from external constraints, the deflected tip forms a precise circular arc (Fig. S5); its curvature–pressure relationship is quantified in the section entitled ‘Relationship between pressure and curvature’. All milli-SRs shown in Fig. 3 are pneumatically actuated via compressed air supplied by a precision syringe pump (Fig. S10).

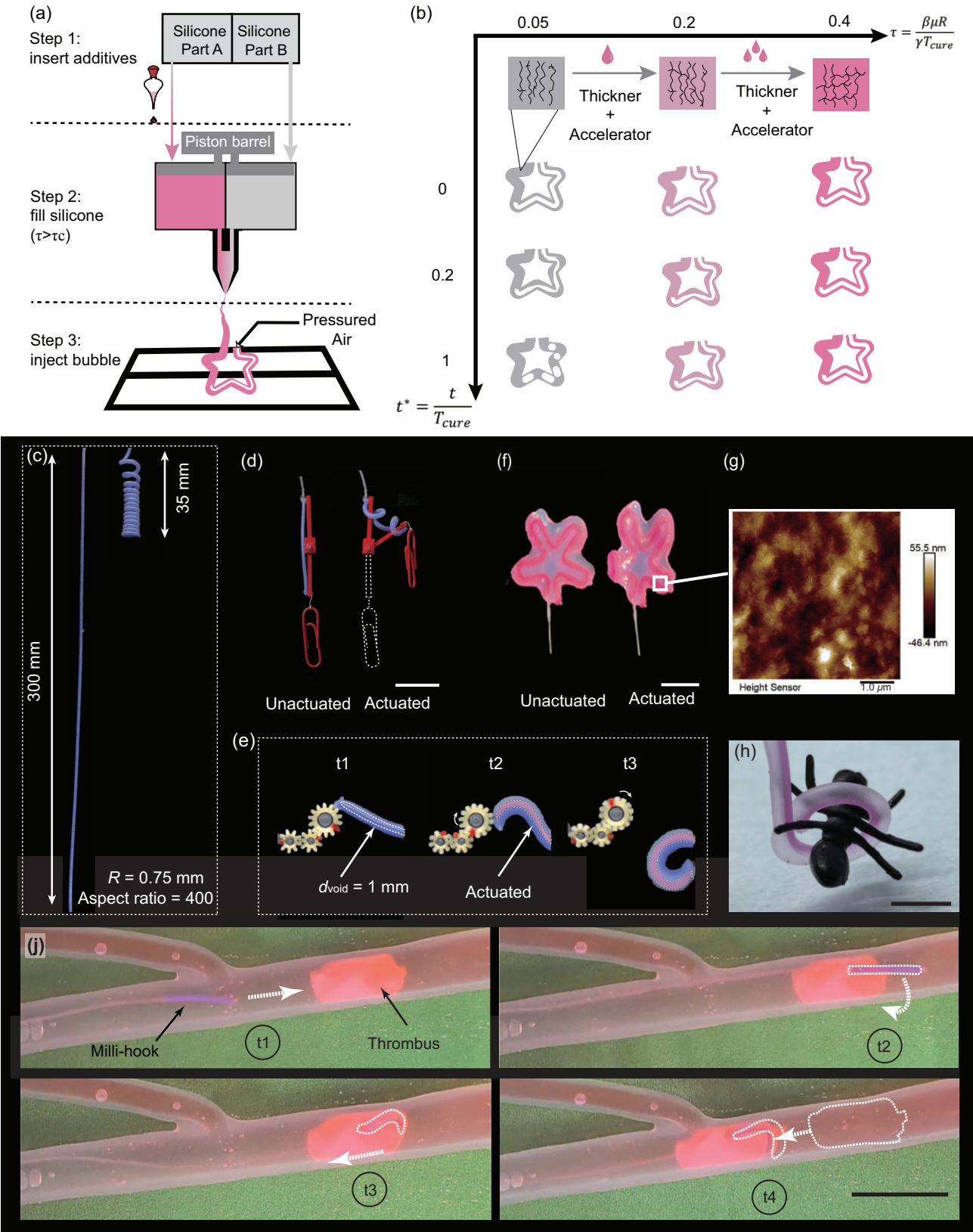


Figure 3. Silicone modification and milli-SRs by mini BC. (a) Silicone modification strategy. (b) The interfacial behaviors as a function of the dimensionless time t/T_{cure} when creating a starlike soft actuator with a diameter of 2 mm. From left to right, we add additives to modify its stability condition τ . (c–e) Soft actuators similar in shape but smaller compared to those produced by bubble casting. (c) Contractile coiling of an actuator with a radius of

Figure 3. (Continued) $R = 0.75$ mm and $L = 300$ mm. (d) Muscle-like contraction of a soft actuator that drives a microscale rotating pair. Scale bar: 5 mm. (e) Series images of bending actuator driving the milli-gear set. (f) A star-like actuator is attached to a thin membrane. Scale bar: 5 mm. (g) The atomic force microscope image of the void surface of the soft actuator. (h) A milli-gripper grasping and holding an ant model. Scale bar: 5 mm. (j) A milli-gripper with a bendable tip enters the vessel (inner diameter of 8 mm) and withdraws a thrombus simulator. Its contour is delineated with a dashed line for enhanced clarity. Scale bar: 10 mm.

Biomedical application

Bronchoscopy is a common procedure for examining lung diseases, using a slender bronchoscope (2.2–6.3 mm) with a micro-camera for clinical evaluation. Its steerable tip, controlled by multiple cables, allows precise navigation through the bronchial tree (Fig. 4a). However, commercial bronchoscopy can cause complications like tissue damage and bleeding. To mitigate these risks, the use of soft materials presents an inherently safer alternative, reducing pain and promoting faster recovery.

Here, we designed an omni-curved bronchoscope tip composed of milli-actuators capable of reaching the quaternary bronchus (Fig. 4b). The tip incorporates three 1.5-mm soft actuators fabricated by mini BC with Dragon Skin 10 (Smooth-On Inc.) and a micro-camera (TA10, 720p, 0.65×0.65 mm²) equipped with two miniature white LEDs. The actuators are arranged in parallel and glued together, with the camera fixed at the tip. Selective pressurization of individual chambers produces localized elongation, inducing deflection of the tip (Fig. S9). For enhanced safety, normal saline is used as the pressurizing fluid in case of accidental explosion. The soft material, with a Young's modulus of less than 150 kPa and demonstrated biocompatibility, minimizes the risk of tissue damage, ensuring that the tip is gentle enough to navigate the bronchial walls without causing harm. It is dexterous with a maximum bending angle of 180° (Fig. S4d) that can meet the need for navigating the bronchus.

To evaluate its potential for biomedical applications, we assess its capabilities to steer and detect in a realistic setting. A real-size, resin bronchus model, which accurately mimics the human bronchial environment, is used for this purpose. The model is transparent to allow for presentation (Fig. 4c). The task of the soft bronchoscope is to insert into the main bronchi ($d = 15$ – 17 mm; Fig. 4c, i), bend to the right into the right lobar bronchi ($d = 4$ – 10 mm; Fig. 4c, ii) and reach the right lower lobar bronchus to examine the subsegmental bronchus ($d = 2$ – 4 mm; Fig. 4c, iii). A number is added at the end of each subsegmental bronchus, and a special marker '+' is glued to the bronchus labeled 1.

The path from the main bronchi to the right lower lobar bronchus spans diameters ranging from 17 to 4 mm, over a distance of 25 cm. In Fig. 4c, iv–ix, we experimentally demonstrate that our soft bronchoscope can complete this task (Movie S8). The

operator holds the soft bronchoscope and manually manipulates the switch to adjust the inner pressure of the milli-actuators. The operator can control the bending of the soft bronchoscope in the desired direction. The micro-camera on the top of the soft bronchoscope detects the marker '+' near the branch labeled 1 in Fig. 4c, iv as well as labels 2–7 in Fig. 4c, v–ix.

DISCUSSION

This work elucidates and suppresses the interfacial instability in bubble casting milli-SRs, thereby pushing the attainable lower bound of the technique to the millimeter regime. Our study reveals that interfacial tension and viscous resistance act as antagonistic regulators of interfacial instability, a coupling previously unreported [37,41,42]. A dimensionless stability condition τ is introduced to predict the onset of instability; guided by it, we further prescribe modification strategies that avert the unstable behavior. Whereas conventional bubble casting focuses on bubble generation, our work centers on instability theory and mitigating bubble instability.

The mini-BC technique explains and eliminates the interfacial instability in bubble casting milli-SRs, thereby broadening the applicability of bubble casting at the millimeter scale. Our study reveals that interfacial tension and viscous resistance generally exert antagonistic effects on interfacial instability when a milli-bubble forms in the silicone liquid, a phenomenon not previously addressed in the literature [37,41,42]. Specifically, we propose the critical stable condition τ to predict the occurrence of interfacial instability and modification strategies to avoid the interfacial instability. This approach facilitates the fabrication of shape-variable soft robots with dimensions an order of magnitude smaller than those previously achieved through bubble casting. We show the utility of milli-SRs in driving micro-mechanics, grasping tiny objects and entering narrow tubes. Notably, we present a significant case of a soft bronchoscope that can navigate complex bronchial structures and perform detecting tasks, underscoring the great potential of mini-BC milli-SRs in the biomedical field.

Given the versatility of mini BC, we aim to extend its applications across other domains within biomedicine in the future. Coupling milli-SRs with novel materials can extend their capabilities beyond

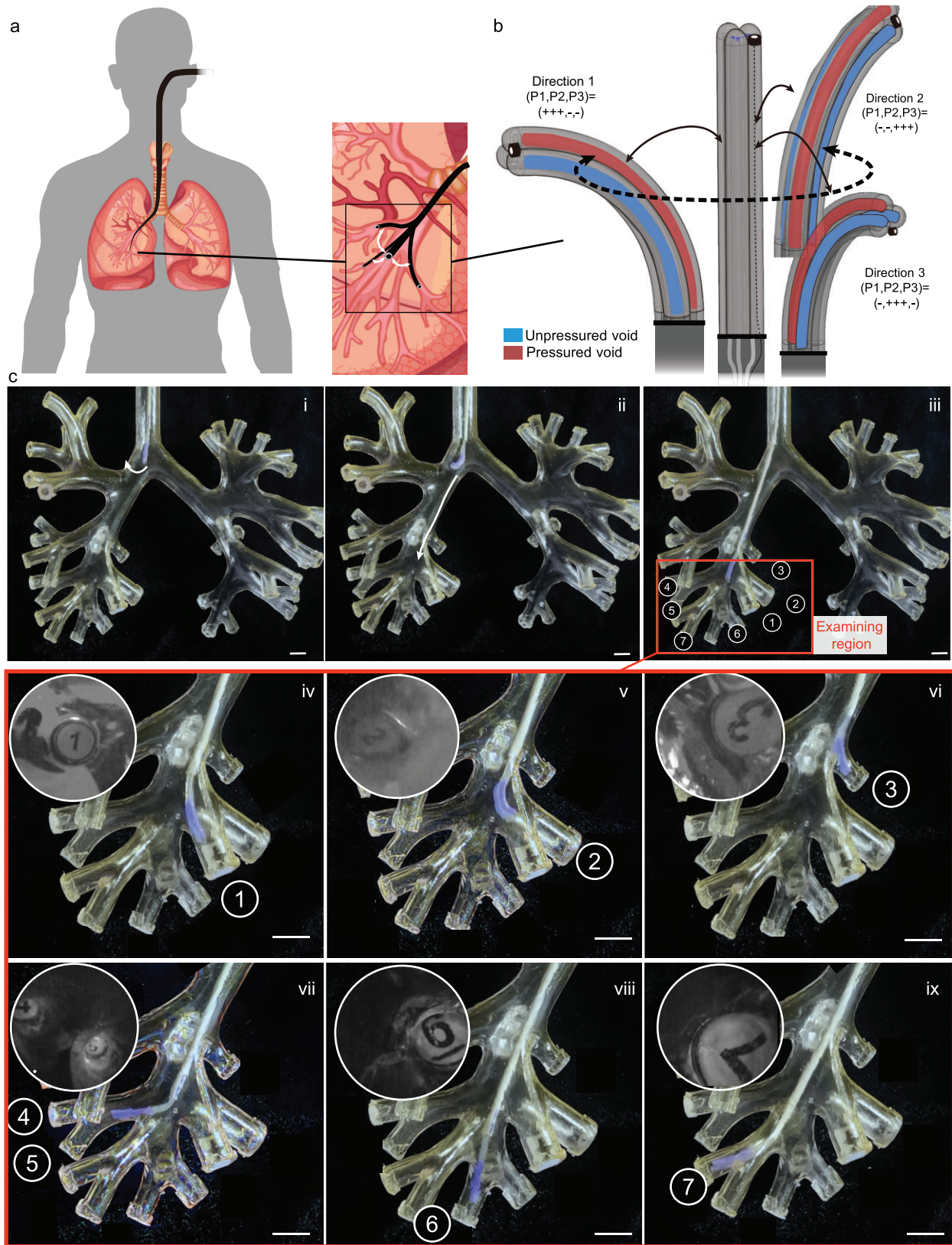


Figure 4. Millimeter-scale soft bronchoscope. (a) Overview of soft bronchoscope steering in the bronchus. (b) The steerable tip has two bending degrees of freedom actuated by three inner pressured voids and the micro-camera captures images from various directions. (c) The soft bronchoscope steers from the trachea (i–ii) to six fourth-order bronchi (iii–ix) and the micro-camera detects the numbered markers visible in the endoscopic view shown in the top-left corner of each subfigure. Scale bars: 5 mm.

single-elastomer designs, such as shape-memory alloys for tunable stiffness and hydrogel coatings for targeted drug elution. Furthermore, integrating *in situ* sensing modules—capable of real-time quantification of temperature, pressure and chemical composition—into milli-SRs constitutes a pivotal strategy for advancing next-generation process intensification. In summary, our mini BC provides a new approach to the design and fabrication of milli-SRs, offering innovative solutions to interfacial instability at the millimeter scale.

METHOD

Stability condition

The stability condition $\tau > \tau_{the}$ can be reformulated as

$$R > \frac{\tau_{th}}{\beta} \frac{\gamma T_{cure}}{\mu} \quad (\text{stable state}), \quad (5)$$

$$R < \frac{\tau_{th}}{\beta} \frac{\gamma T_{cure}}{\mu} \quad (\text{unstable state}). \quad (6)$$

We mark the stable state with pink and the unstable state with gray in Fig. 2e. A linear classifier can separate them with a slope $\tau_{th}/\beta = 9.1 \times 10^{-4}$. Therefore, the threshold criterion can be calculated as $\tau_{th} = 0.3$.

Silicone modification

We modify the dual-component platinum cure liquid silicone that is most commonly used in soft robotics labs. To enhance the class of liquid silicone, such as Dragon Skin 10, Platinum Silicone Cure Accelerator (Plat-Cat) and Thixotropic Agent (Thi-Vex) are chosen. For other kinds of commercial silicone, the corresponding accelerator and thickener can be obtained from silicone suppliers. Additives (Plat-Cat and Thi-Vex) are mixed into part A of Dragon Skin 10 at weight ratios of 1:20 and 1:100, respectively, using a glass stirring rod. The mixture is then transferred to the left chamber of the cartridge. Subsequently, part B is poured into another cartridge part, and the silicone cartridge undergoes defoaming in a vacuum chamber (-95 kPa, 20 min). The evacuation rate should be no more than 10 Pa/s in case of liquid spillage. Following defoaming, we seal the modified silicone into a cartridge with pistons. To mitigate the adverse effects of phase separation in silicone, the sealed cartridge should be stored in a horizontal position to maintain component homogeneity during extrusion. Storage should be at room temperature (73°F or 23°C) away from direct sunlight. To preserve rheological stability, the material should be used within two weeks.

Injection system

The injection system includes a two-component cartridge gun (MPD50, COX Inc.), cartridges (50 + 50 ml, Runze Inc.) and mixing nozzles (F1 XL3.2-16S, Runze Inc.). After installing the mixing nozzle on the cartridge, the cartridge is placed into the gun. Once the gun is triggered, 400 kPa of pressure is applied to extrude both silicone parts into the mixing nozzle in a common weight of 1:1. The initial portion of silicone extruded is recommended to be discarded to avoid issues arising from non-uniform ratios. We connect the nozzle exit and the mold with an elastic silicone tube.

Rheological protocols

The viscosity of the silicone liquid is characterized by a rotational rheometer (Discovery Hybrid rheometer, TA Instruments Inc.) equipped with a parallel plate. The sample is freshly extruded silicone from the injection system that is thoroughly mixed prior to sampling. The surface tension of the silicone was determined using the drop weight method, with measurements conducted on OCA25 (Dataphysics Instruments Inc.).

Fabrication of the milli-hooker

We fabricate the milli-hooker with silicone (Dragon Skin 10, Smooth on Inc.) in a tubular mold with a diameter of 1.5 mm and a length of 100 mm. The silicone is modified by inserting thickener and accelerator. We propel the bubble in the liquid silicone to the waiting point M and segment #1 forms and rises under buoyancy (Fig. S7a). After a waiting time, we propel the bubble to the outlet to form segment #2 of the bubble. The silicone molecules have undergone cross-linking, preventing segment #2 from rising (Fig. S7b). Upon curing, the axially variable void enables the milli-actuator to deform into a hook-like shape (Fig. S7c).

SUPPLEMENTARY DATA

Supplementary data are available at [NSR](https://doi.org/10.1093/nsr/nwaf413) online.

FUNDING

This work was supported in part by the National Natural Science Foundation of China (52025057, T2293725 and 52305029), the National Key R&D Program of China (2024YFB4707504), the Science and Technology Commission of Shanghai Municipality (24511103400) and an Xplorer Prize.

AUTHOR CONTRIBUTIONS

R.B., N.Z. and G.G. designed the research; R.B., N.Z. and X.Y. performed the research; G.G. supervised the research; R.B. wrote the manuscript. All authors discussed, reviewed and edited the manuscript.

Conflict of interest statement. None declared.

REFERENCES

- Kim Y, Parada GA, Liu S *et al.* Ferromagnetic soft continuum robots. *Sci Robot* 2019; **4**: eaax7329.
- Yan Y, Wang T, Zhang R *et al.* Magnetically assisted soft millirobots for occluded lumen morphology detection. *Sci Adv* 2023; **9**: eadi3979.
- Thai MT, Phan PT, Tran HA *et al.* Advanced soft robotic system for in situ 3D bioprinting and endoscopic surgery. *Adv Sci* 2023; **10**: e2205656.
- Kim Y, Genevriere E, Harker P *et al.* Telerobotic neurovascular interventions with magnetic manipulation. *Sci Robot* 2022; **7**: eabg9907.
- Hu W, Lum GZ, Mastrangeli M *et al.* Small-scale soft-bodied robot with multimodal locomotion. *Nature* 2018; **554**: 81–5.
- Wu Y, Dong X, Kim J *et al.* Wireless soft millirobots for climbing three-dimensional surfaces in confined spaces. *Sci Adv* 2022; **8**: eabn3431.
- Zhang Y, Yang D, Yan P *et al.* Inchworm inspired multimodal soft robots with crawling, climbing, and transitioning locomotion. *IEEE Trans Robot* 2022; **38**: 1806–19.
- Van Lewen D, Janke T, Lee H *et al.* A millimeter-scale soft robot for tissue biopsy procedures. *Adv Intell Syst* 2023; **5**: 2200326.
- Roh Y, Kim M, Won SM *et al.* Vital signal sensing and manipulation of a microscale organ with a multifunctional soft gripper. *Sci Robot* 2021; **6**: eabi6774.
- Bian R, Zhang N, Yang X *et al.* A variable stiffness soft actuator with a center skeleton and pin-socket jamming layers. In: Liu H, Yin Z, Liu L *et al.* (eds.) *Intelligent Robotics and Applications. ICIRA 2022*. Cham: Springer, 2022, 325–32.
- Yang Z, Xu C, Lee JX *et al.* Magnetic miniature soft robot with reprogrammable drug-dispensing functionalities: toward advanced targeted combination therapy. *Adv Mater* 2024; **36**: 2408750.
- Phan PT, Thai MT, Hoang TT *et al.* Hfam: Soft hydraulic filament artificial muscles for flexible robotic applications. *IEEE Access* 2020; **8**: 226637–52.
- Li Y, Peine J, Mencattelli M *et al.* A soft robotic balloon endoscope for airway procedures. *Soft Robot* 2022; **9**: 1014–29.
- Diwakar N and Miloh T *et al.* AC electrohydrodynamic propulsion and rotation of active particles of engineered shape and asymmetry. *Curr Opin Colloid Interface Sci* 2022; **59**: 101586.
- Lee S, Moghani M, Li A *et al.* A small steerable tip based on dielectric elastomer actuators. *IEEE Robot Autom Lett* 2023; **8**: 6531–8.
- Dong Y, Wang L, Zhang Z *et al.* Endoscope-assisted magnetic helical micromachine delivery for biofilm eradication in tympanostomy tube. *Sci Adv* 2022; **8**: eabq8573.
- Deng B, Chen L, Wei D *et al.* Pulse-driven robot: motion via solitary waves. *Sci Adv* 2020; **6**: eaaz1166.
- Son D, Ugurlu MC, Sitti M. Permanent magnet array-driven navigation of wireless millirobots inside soft tissues. *Sci Adv* 2021; **7**: eabi8932.
- Chen X, Goodnight D, Gao Z *et al.* Scaling up nanoscale water-driven energy conversion into evaporation-driven engines and generators. *Nat Commun* 2015; **6**: 7346.
- Fusi G, Del Giudice D, Skarsetz O *et al.* Autonomous soft robots empowered by chemical reaction networks. *Adv Mater* 2023; **35**: 2209870.
- Wang H, Gao J, Xu C *et al.* Light-driven biomimetic nanomotors for enhanced photothermal therapy. *Small* 2024; **20**: 2306208.
- Ahmed S, Wang W, Bai L *et al.* Density and shape effects in the acoustic propulsion of bimetallic nanorod motors. *ACS Nano* 2016; **10**: 4763–9.
- Gu G, Zhang N, Xu H *et al.* A soft neuroprosthetic hand providing simultaneous myoelectric control and tactile feedback. *Nat Biomed Eng* 2021; **5**: 589–98.
- Polygerinos P, Correll N, Morin SA *et al.* Soft robotics: review of fluid-driven intrinsically soft devices; manufacturing, sensing, control, and applications in human-robot interaction. *Adv Eng Mater* 2017; **19**: 100016.
- Yang D, Feng M, Sun J *et al.* Soft multifunctional bistable fabric mechanism for electronics-free autonomous robots. *Sci Adv* 2025; **11**: eads8734.
- Zhang N, Ren J, Dong Y *et al.* Soft robotic hand with tactile palm-finger coordination. *Nat Commun* 2025; **16**: 2395.
- Yang X, Zhang N, Huang X *et al.* Multidirectional bending soft pneumatic actuator with fishbone-like strain-limiting layer for dexterous manipulation. *IEEE Robot Autom Lett* 2024; **9**: 3815–22.
- Kalmar M, Boese A, Landes R *et al.* Injection and infusion technology disruption for use in MRI. *Med Dev* 2019; **12**: 469–78.
- Fu S, Dong S, Shen H *et al.* Multifunctional magnetic catheter robot with triaxial force sensing capability for minimally invasive surgery. *Research* 2025; **8**: 0681.
- Shah A and Aran S. A review of magnetic resonance (mr) safety: the essentials to patient safety. *Cureus* 2023; **15**: e47345.
- Ceron S, Gardi G, Petersen K *et al.* Programmable self-organization of heterogeneous microrobot collectives. *Proc Natl Acad Sci USA* 2023; **120**: e2221913120.
- Yan Y, Wang T, Zhang R *et al.* Magnetically assisted soft millirobots for occluded lumen morphology detection. *Sci Adv* 2023; **9**: eadi3979.
- Dong X, Luo X, Zhao H *et al.* Recent advances in biomimetic soft robotics: fabrication approaches, driven strategies and applications. *Soft Matter* 2022; **18**: 7699–734.
- Haouas W, Gauthier M, Rabenorosoa K. Miniaturized soft robotics: recent advances and futures opportunities. *Curr Robot Rep* 2024; **5**: 15–27.
- Chi Y, Zhao Y, Hong Y *et al.* A perspective on miniature soft robotics: actuation, fabrication, control, and applications. *Adv Intell Syst* 2023; **6**: 20063.
- Purcell EM. Life at low Reynolds number. *Am J Phys* 1977; **45**: 3–11.

37. Fan D, Yuan X, Wu W *et al.* Self-shrinking soft demoulding for complex high-aspect-ratio microchannels. *Nat Commun* 2022; **13**: 32859.
38. Duraivel S, Laurent D, Rajon DA *et al.* A silicone-based support material eliminates interfacial instabilities in 3D silicone printing. *Science* 2023; **379**: 1248–52.
39. Li J, Cao J, Bian R *et al.* Multimaterial cryogenic printing of three-dimensional soft hydrogel machines. *Nat Commun* 2025; **16**: 185.
40. Ji M, Li Q, Cho IH *et al.* Rapid design and analysis of microtube pneumatic actuators using line-segment and multi-segment Euler-Bernoulli beam models. *Micromachines* 2019; **10**: 780.
41. Jones TJ, Jambon-Puillet E, Marthelot J *et al.* Bubble casting soft robotics. *Nature* 2021; **599**: 229–33.
42. Becker K, Teeple C, Charles N *et al.* Active entanglement enables stochastic, topological grasping. *Proc Natl Acad Sci USA* 2022; **119**: e2209819119.
43. Guo X, Tang W, Qin K *et al.* Powerful UAV manipulation via bioinspired self-adaptive soft self-contained gripper. *Sci Adv* 2024; **10**: eadn6642.
44. Bretherton FP. The motion of long bubbles in tubes. *J Fluid Mech* 1961; **10**: 166–88.
45. Tsai TM and Miksis MJ. Dynamics of a drop in a constricted capillary tube. *J Fluid Mech* 1994; **274**: 197–217.
46. Olbricht WL and Kung DM. The deformation and breakup of liquid drops in low Reynolds number flow through a capillary. *Phys Fluids A* 1992; **4**: 1347–54.
47. Jang Y, Nabaee H, Suzumori K. Effects of surface roughness on direct plasma bonding between silicone rubbers fabricated with 3D-printed molds. *ACS Omega* 2022; **7**: 45004–13.